VII International Conference on Computational Methods in Marine Engineering
MARINE 2017
M. Visonneau, P. Queutey and D. Le Touzé (Eds)

NUMERICAL INVESTIGATION OF STRONG ADDED MASS EFFECT FOR FLUID-STRUCTURE CALCULATIONS APPLIED TO MOVING HYDROFOILS

Emmanuel LEFRANÇOIS

Roberval Laboratory CNRS UMR 7337
Sorbonne Universités - Université de Technologie de Compiègne
CS 60319, 60203 Compiègne, France
e-mail: emmanuel.lefrancois@utc.fr

Key words: 2D Panel Method, fluid structure interaction, hydrofoil dynamics, added mass

Abstract. This paper presents a corrected partitioned scheme for investigating fluid-structure interaction (FSI) that may be encountered by lifting devices immersed in heavy fluid such as liquids. The purpose of this model is to counteract the penalizing impact of the added mass effect on the classical partitioned FSI coupling scheme. This work is based on an added mass corrected version of the classical strongly coupled partitioned scheme presented in [1]. Results show that this corrected version systematically allows convergence to the coupled solution with no dependency on fluid density . The fluid flow model considered here uses a non-stationary potential approach, commonly termed the Panel Method. The advantage of this kind of approach is twofold: first, in restricting itself to a boundary method and, second, in allowing an added mass matrix to be estimated as a post-processing phase.

1 CONTEXT AND INTEREST OF THIS STUDY

The research presented in this article focuses on the development of a numerical tool for investigating fluid-structure interactions (FSI) between a fluid flow that is not confined (infinite) and a current turbine with blades. Many similarities may be observed from its aerial version (wind-mill) but a major point of concern results from a fluid density 800 times higher than in the air. The constant search for an optimal solution (by increasing size and reducing mass) inevitably leads to flexible behavior resulting from hydrodynamic loads, and this flexible behavior may have serious impacts on the efficiency of the device.

Since simplifying is part of the process of understanding, the FSI model may here without loss of generality be restricted to a 2D airfoil placed in a flow and having two degrees of freedom (*dof*), namely plunging and pitching motions. This assumption is justified by the fact that the physical phenomena that occur around the cross-flow section of a blade are quite similar to those encountered by lifting airfoils in two dimensions (2D). The *Panel Method* approach [2, 3] is of particular interest for fluid flow calculations around lifting device due to the fact it has been originaly designed for. This potential approach is restricted to incompressible and irrotational

flows, however if completed by a Kutta condition, it can be extended to lifting flows. The FSI approach is here based on a *partitioned* coupling with a dedicated solver for each of the two physics (namely fluid flow and structure dynamics). Exchanges take place regularly between the two solvers via a coupling scheme [4, 5] that is based on successive solutions produced by the fluid and structure solvers. The coupling is said to be *loosely coupled partitioned* if only one shot (that is to say a single computation) per time step is required for each field, and *strongly coupled partitioned* if an iterative procedure is used to ensure convergence of the coupled solution [6]. In an industrial context, the biggest advantage that partitioned coupling has over monolithic coupling (with a single solver) is the modularity of the approach, which makes the different solvers much easier to implement and allows distributed computation. The major drawback of the *standard* partitioned FSI coupling scheme is that where higher density fluids are involved (meaning strong effects of added mass), convergence is no longer guaranteed, and divergence will generally be observed, regardless of the chosen time step for incompressible flows [7]. A number of approaches have been proposed since the last decade to counter this drawback including semi-implicit discretization [8] and adaptive Aitken under-relaxation [9], but convergence is not always guaranteed, or may be slow in cases of high-density fluids such as blood or water. Our objective in this paper is to show that in order to take into account heavy fluid flows such as in sea currents, the coupling scheme must be corrected, as described for example in [1], in order to counteract the penalizing impact of the added mass effect on the classical FSI coupling scheme. This correction is based on estimating an added mass matrix $[M^e_{add}]$ that may considerably improve and/or ensure the iterative phase of a strongly coupled partitioned approach. Moreover, the interest of an approach such as the Panel Method is here twofold, in that it enables this matrix to be estimated in a post-processing process without the use of a fluid mesh: this constitutes a serious and solid advantage.

2 MATHEMATICAL MODELS

2.1 Dynamics for a hydrofoil with two degrees of freedom

Here we consider a 2D airfoil with chord length c, of mass m and flexibly attached to a fixed point, as illustrated in Figure 1. We have the pivot point P (also called the elastic axis), the aerodynamic center F (located at $c/4$ from the leading edge) and the center of mass location G. Two *dof* are here considered, namely plunging $w(t)$ and a pitching $\theta(t)$ motions. The vertical and rotational components of the airfoil velocity are respectively denoted by V_G and $\dot{\theta}$.

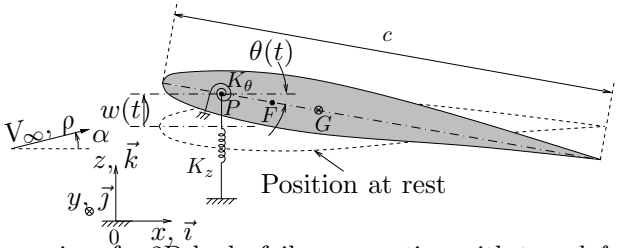

Figure 1: Dynamics of a 2D hydrofoil cross section with two *dof* $w(t)$ and $\theta(t)$

The fundamental equations may be obtained from the kinetic and potential energy of the

airfoil:

$$\mathcal{E}_k = \frac{1}{2}\left(mV_G^2 + \mathcal{I}|_G\,\dot{\theta}^2\right) \quad \text{and} \quad \mathcal{E}_p = \frac{1}{2}\left(K_z w^2 + K_\theta \theta^2\right) - PG\,mg\,\theta,$$

with K_z denoting the axial rigidity along the $z-$axis, K_θ the torsional rigidity with respect to the $y-$axis and $\mathcal{I}|_G$ the mass moment of inertia about G. From Lagrange's equation we then obtain the set of two equations:

$$\begin{bmatrix} m & -mPG \\ -mPG & \mathcal{I}_P \end{bmatrix} \begin{Bmatrix} \ddot{w} \\ \ddot{\theta} \end{Bmatrix} + \begin{bmatrix} K_z & 0 \\ 0 & K_\theta \end{bmatrix} \begin{Bmatrix} w \\ \theta \end{Bmatrix} = \begin{Bmatrix} \mathcal{R}_z \\ \mathcal{M}|_P + PG\,mg \end{Bmatrix} \tag{1}$$

where $\mathcal{R}_z$ and $\mathcal{M}|_P$ denote respectively the vertical component of the generalized force obtained from the pressure integration, and the resulting pitching moment at P. Finally, this may be condensed to the following:

$$[M]\{\ddot{U}\} + [K]\{U(t)\} = \{F_p(t)\}, \text{ with } \{U(0)\} = \{U^0\} \text{ and } \{\dot{U}(0)\} = \{0\}, \tag{2}$$

where $[M]$ and $[K]$ denote respectively the mass and the rigidity matrices corresponding to the attachment of the airfoil, and $\{U\}$ denotes the two dof. The term $\{F_p\}$ denotes for the sollicitation vector resulting from aerodynamic loads.

2.2 Panel Method (PM) for lifting potential flows

Panel methods are particularly suitable for calculating the flow field over an airfoil that undergoes unsteady time-dependent motion in a fluid that may be assumed inviscid and incompressible. Let φ define the total potential such that $\overrightarrow{V} = \overrightarrow{\nabla}\varphi$. Combining this with the first of the two equations just cited, we obtain the classical Poisson equation $\Delta\varphi = 0, \quad \forall \vec{x} \in \mathcal{V}$.

The main idea in the Panel Method is not to solve this Laplacian equation in the classical way for the entire fluid domain, but to cast the same analysis in a boundary integral equation form for which [10], where the Hess & Smith Panel Method (HSPM) was introduced, is considered to be the reference paper. In this approach, with 2D non-stationary flows being restricted as set out in [11], the velocity $\overrightarrow{V}$ at any point $\vec{x} = (x,\, z)$ of the fluid domain is decomposed according to:

$$\overrightarrow{V}(\vec{x}) = \overrightarrow{V}_\infty + \vec{v} \quad \text{with} \quad \vec{v} = \oint_S \frac{\sigma(s)\vec{r}}{2\pi r^2} ds + \oint_S \frac{\tau(s)}{2\pi r}\vec{e}_\theta ds, \tag{3}$$

where $\overrightarrow{V}_\infty$ defines the velocity of the uniform flow at infinity. The vector $\vec{v}$ denotes the disturbance field due to the airfoil and results from two contributions, since the airfoil may be represented by two elementary flows (also called singularities) corresponding to source flow ($\sigma(s)$) and vortex flow [11] ($\tau(s)$). This expression satisfies the irrotationality condition and the boundary condition at infinity that stipulates the cancellation of the disturbance velocity, and it results from Green's identity (we refer to [2] for a complete mathematical analysis). For a given set of source strength $\sigma(s)ds$ and vortex strength $\tau(s)ds$ (assumed uniform on the airfoil), it is then theoretically possible to define the velocity field at any point of the fluid domain: in the approach adopted in [10], the vortex strength $\tau(s)$ is taken to be constant on the airfoil and adjusted to satisfy a lifting condition.

For points belonging to the interface between the flow and the airfoil, the boundary condition that stipulates no flow through surface enables us to define a given set of equations to be solved for $\sigma(s)$. Completed by the Kutta condition that stipulates that the flow must leave the trailing edge smoothly, the set to be solved for $\sigma(s)$ and τ is now complete.

In order to couple the fluid flow with the structure, we need to know the pressure p. This may be calculated at any point using the non-stationary form of Bernoulli's equation [12].

$$p + \rho g z + \rho \frac{V^2}{2} + \rho \frac{\partial \varphi}{\partial t} = f(t).$$

3 NUMERICAL MODELS

3.1 Structure model

The time resolution of equation (2) is here obtained using a Newmark-Wilson finite difference [13] scheme such as:

$$\left(\frac{4}{\Delta t^2}[M] + [K] \right) \{\Delta U\} = \{F_p\}^n - [K]\{U\}^n + [M] \left(\frac{4}{\Delta t}\{\dot{U}\}^n + \frac{1}{4}\{\ddot{U}\}^n \right). \tag{4}$$

The indexes n and $n+1$ correspond to the times t and $t + \Delta t$ and $\{\Delta U\} = \{U\}^{n+1} - \{U\}^n$. It should be pointed out that the fluid load term $\{F_p\}$, resulting from fluid pressure integration on the airfoil, is here computed at time step n because of the partitioned nature of the coupling scheme that we are considering. The mechanical energy can be calculated for each time step and is divided into two parts, respectively kinetic and potential:

$$\mathcal{E}_m = \mathcal{E}_k + \mathcal{E}_p \quad \text{with} \quad \mathcal{E}_k = \frac{1}{2} < \dot{U} > [M]\{\dot{U}\}, \quad \mathcal{E}_p = \frac{1}{2} < U > [K]\{U\}. \tag{5}$$

3.2 Fluid model

The fluid flow numerical model is built in accordance with [11]. It first requires the discretization of the airfoil that is decomposed (see Figure 2) with N *panels* for $N+1$ nodes (symbol $\circ$). Each panel i is defined by a pair of boundary points, (x_i, z_i) and (x_{i+1}, z_{i+1}), and a *control point* (cp_i) located at the midpoint (symbol $\times$).

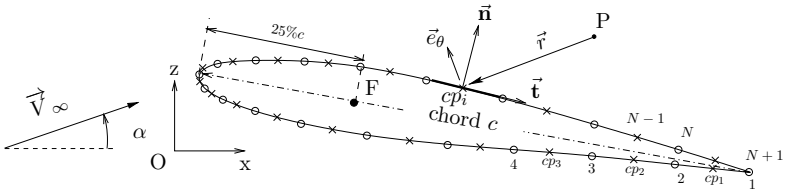

Figure 2: Panel representation of the airfoil surface

The vectors $\vec{\mathbf{n}}_i$ and $\vec{\mathbf{t}}_i$ located at control point i denote respectively the normal and the tangential vectors. The perimeter of the airfoil is denoted as l.

3.2.1 Stationary form

The fluid velocity at any point in the fluid domain is obtained by integrating equations (3) on the airfoil surface. This integration involves summing all panel contributions such that:

$$\overrightarrow{V}(P) = V_\infty \vec{\imath} + V_\infty \vec{k} + \vec{v} \quad \text{where} \quad \vec{v} = \sum_{j=1}^{N} \int_{Lj} \frac{\sigma_j \vec{r}}{2\pi r^2} ds + \sum_{j=1}^{N} \int_{Lj} \frac{\tau}{2\pi r} \vec{e}_\theta ds \tag{6}$$

For each control point i, with the boundary condition of non-penetrating flow, integration yields the following expression:

$$(V_\mathbf{n})_i = \vec{V}_\infty . \vec{\mathbf{n}}_i + \sum_{j=1}^{N} A_{ij}^\mathbf{n} \sigma_j + \tau \sum_{j=1}^{N} B_{ij}^\mathbf{n} = 0, \quad i = 1, \ldots, N \tag{7}$$

The terms $A_{ij}^\mathbf{n}$ and $B_{ij}^\mathbf{n}$, detailed in [11], are the influence cœfficients for the source and vorticity distributions: the first subscript i denotes the panel that is subject to the influence of the panel indexed by j.

In order to ensure the lifting capability of the airfoil, we here consider a Kutta-Joukowski condition stipulating that the magnitude of the two tangential velocities at the trailing edge (control point 1 and N) must be equal to each other:

$$(V_\mathbf{t})_N = -(V_\mathbf{t})_1 \quad \text{with} \quad (V_\mathbf{t})_i = \vec{V}_\infty . \vec{\mathbf{t}}_i + \sum_{j=1}^{N} A_{ij}^\mathbf{t} \sigma_j + \tau \sum_{j=1}^{N} B_{ij}^\mathbf{t}, \tag{8}$$

The minus sign results from the fact that the two tangential vectors $\vec{\mathbf{t}}_1$ and $\vec{\mathbf{t}}_N$ are opposite. The overall system that needs to be solved comes out of equations (7) and (8), and may be written:

$$\begin{bmatrix} & \vdots & \\ A_{i1}^\mathbf{n} & .. & A_{iN}^\mathbf{n} & \sum B_{ij}^\mathbf{n} \\ & \vdots & \\ (A_{11}^\mathbf{t} + A_{N1}^\mathbf{t}) & .. & (A_{1N}^\mathbf{t} + A_{NN}^\mathbf{t}) & \sum (B_{1j}^\mathbf{t} + B_{Nj}^\mathbf{t}) \end{bmatrix} \begin{Bmatrix} \sigma_1 \\ \vdots \\ \sigma_N \\ \tau \end{Bmatrix} = \begin{Bmatrix} \vdots \\ -\vec{V}_\infty . \vec{\mathbf{n}}_i \\ \vdots \\ -\vec{V}_\infty . (\vec{\mathbf{t}}_1 + \vec{\mathbf{t}}_N) \end{Bmatrix}$$

Solving this system allows the pressure to be computed at all control points, using the following:

$$p_i = \rho \frac{V_\infty^2}{2} C_{pi} \quad \text{with} \quad C_{pi} = 1 - \left(\frac{(V_t)_i}{V_\infty} \right)^2, \tag{9}$$

where C_{pi} denotes the nodal pressure cœfficient.

3.3 Non-stationary form

According to Kelvin's circulation theorem [12], the circulation Γ around a closed curve $\mathcal{C}_1$ (composed of the same fluid particles) moving with the fluid, remains constant with time. Stated mathematically:

$$\Gamma_{\mathcal{C}_1}|_{t=0} = \oint_{\mathcal{C}_1} \overrightarrow{V} . \overrightarrow{ds} = 0 \quad \Rightarrow \quad \frac{d\Gamma_{\mathcal{C}_1}}{dt} = 0, \ \forall t \geq 0$$

The lifting process around an airfoil is directly related to a circulation, in accordance with the Kutta-Joukowsky theorem. We deduce that any changes in the airfoil circulation must be balanced by an equal and opposite change in the wake, resulting from the vortex shedding at the trailing edge of the airfoil.

At time step $(n+1)$, the vortex shedding has a corresponding additional wake element indexed by $_w$, of uniform vorticity τ_w^{n+1} and length Δ^{n+1} such that:

$$\Theta^{n+1} = \tan^{-1}\left(\frac{v_w^{n+1}}{u_w^{n+1}}\right), \quad \Delta^{n+1} = \Delta t\sqrt{(u_w^{n+1})^2 + (v_w^{n+1})^2}, \tag{10}$$

where $(u_w,\, v_w)$ denote the velocity components at the trailing edge and

$$\tau_w^{n+1}\Delta^{n+1} = \Gamma^n - \Gamma^{n+1} = l\left(\tau^n - \tau^{n+1}\right). \tag{11}$$

Each time step n is then associated with a detached vortex n of circulation $\Gamma^n = \tau_w^n\, l$ convected downstream (see Figure 3) by the fluid velocity field.

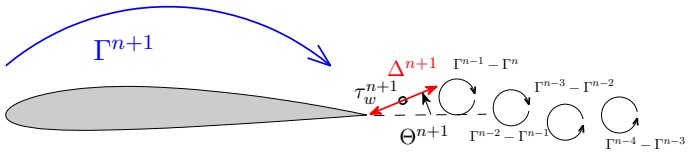

Figure 3: Vortex shedding at trailing edge developed from a shed vorticity panel (τ_w^{n+1},Δ^{n+1})

The non-stationary form of the original equation (7) is then completed by unsteady effects and rearranged using the terms from equation (11) such that:

$$\begin{aligned}\sum_{j=1}^{N} A_{ij}^{\mathbf{n}}\sigma_i^{n+1} \;=\; & \tau^{n+1}\left(\frac{l}{\Delta^{n+1}}(B_{iw}^{\mathbf{n}})^{n+1} - \sum_{j=1}^{N} B_{ij}^{\mathbf{n}}\right) - (\vec{V}_{ST}.\vec{\mathbf{n}}_i)^{n+1} \\ & -\tau^{n}\frac{l}{\Delta^{n+1}}(B_{iw}^{\mathbf{n}})^{n+1} - \sum_{m=1}^{n}(C_{im}^{\mathbf{n}})^{n}\left(\Gamma^{m-1}\text{–}\Gamma^{m}\right).\end{aligned} \tag{12}$$

The term $\vec{V}_{ST}$ denotes the unsteady upstream velocity seen from a coordinate system attached to the airfoil in order to carry the airfoil motion [11] over to the relative fluid velocity calculation such as:

$$\vec{V}_{ST} = \vec{V}_{\infty} - \dot{w}\vec{k} + \dot{\theta}\vec{j}\wedge(\vec{r} - \vec{r}_P), \tag{13}$$

with $\dot{w}$ the vertical velocity component of the airfoil, $\dot{\theta}$ its rotational velocity and P its rotation axis (see Figure 1). The resulting algebraic equations can be written in the form:

$$[\mathcal{A}]\{\sigma\}^{n+1} = \tau^{n+1}\{\mathcal{B}\} + \{\mathcal{C}\}. \tag{14}$$

Vectors $\{\mathcal{B}\}$ and $\{\mathcal{C}\}$ directly depend on the shed vorticity panel values (Δ^{n+1}, Θ^{n+1}, τ_w^{n+1}) and consequently an iterative procedure must be set up to solve the system (14).

3.4 Incorporating added mass effects into the fluid-structure coupling scheme

The coupling process is required to perform FSI calculations in order to regularly update the variables common to both the fluid and the structure solvers. The exchange process should be read as follows:

1 Starting at time n, a single time step is executed in order for the structure solver to update displacements and velocities, bringing us to time $n+1$.

2 The information based on the new structure state is transferred to the fluid code.

3 Starting at time n, a single time step is executed to update all fluid data, bringing us to time $n+1$.

4 The pressure field is transferred to the structure code.

... Steps [1→4] are executed iteratively until some convergence criterion is satisfied.

In order to better counteract the added mass effect that results from heavy fluid flow such as in a liquid (sea currents) and that may lead to divergence, here we propose correcting the classical FSI coupling scheme in relation to the added mass effect. The main idea (in the case of conservative systems only) is that if the real added mass matrix $[M_{add,f}]$ could be calculated exactly, the force term appearing in equation (2) would be exactly replaced by:

$$\{F_p\}^i \equiv -[M_{add,f}]\{\ddot{U}\}^i. \tag{15}$$

For most cases, the real added mass matrix $[M_{add,f}]$ is out of reach. The classical partitioned coupling scheme (denoted by CLAS) is then modified in accordance with [1], and equation (2) is now related to the corrected scheme (denoted by CORR):

$$([M]+[M_{add,e}])\{\ddot{U}\}^{i+1}+[K]\{U\}^{i+1}=\{F_p\}^i+[M_{add,e}]\{\ddot{U}\}^i, \tag{16}$$

where i and $i+1$ are indexes for the iterative process, and $[M_{add,e}]$ is the matrix corresponding to the *estimated* added mass effect resulting from the pressure load all around the structure. Each component $M_{add,e}(i,j)$ is related to *the force on the body in the i-axis resulting from a unit acceleration along the j-axis*. At convergence, the two additional terms cancel out and we get back to the original form of the coupling equation (2). Adding extra terms on both parts of the original equation, in accordance with equation (15), helps to reduce the penalizing effect of $\{F_p\}$ and to increase the beneficial effect of $[M]\{\ddot{U}\}$ on the convergence process. The added mass matrix calculation is calculated according to [14]:

$$M_{add,e}(j,k)=\rho\iiint_V \varphi_{i,k}\varphi_{j,k}dV=\rho\oiint_S \varphi_i\frac{\partial\varphi_j}{\partial n}dS. \tag{17}$$

The above expression is fully compatible with the Panel Method in computing φ_j, the gradient term simply being equal to the normal component of the parietal velocity of the body (a variable that is already known, transmitted by the structure solver).

4 RESULTS

4.1 Thrust generation by a forced oscillating airfoil

This first example is simply intended as a qualitative, graphical illustration of the capability of the Panel Method in relation to the well-known effect of thrust generation through airfoil oscillation (as presented in [11]). The same non-symmetric NACA 2412 airfoil is moved along its plunging and pitching directions, according to:

$$w(t) = w_o \sin(\omega t), \quad \theta(t) = \theta_o \sin(\omega t + \phi)$$

where ϕ introduces a phase shift between the two variables. The unsteadiness in the flow is defined by the reduced frequency $\kappa = \dfrac{\omega c}{V_\infty}$: two different non-stationary calculations are conducted respectively for $\kappa = 0.5$ and $\kappa = 2$. The entire simulation takes place over eight periods of oscillation with 200 time steps per period. The airfoil (chord unity) is placed in a flow with $V_\infty = +5\,m/s$, $w_o = 0.2\,m$, $\theta_o = 8^o$ and $\phi = 60^o$ and the airfoil is decomposed into 105 panels.

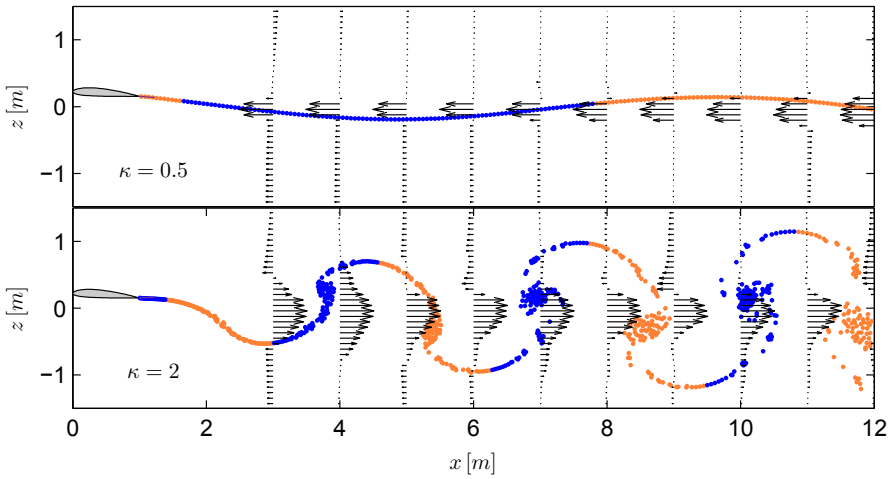

Figure 4: Different flow characterizations according to the reduced frequency κ

Results of the two calculations are illustrated in Figure 4. In each case a wake appears that results from the successive generation of vortex shedding at the trailing edge of the airfoil. For different stations ($x = 3, \ldots, 11\,m$) downstream of the trailing edge, the time-averaged velocity profile (reduced from the value u_∞) is superposed. The two cases clearly show opposing behaviors: in the first case ($\kappa = 0.5$), the wake contributes to the airfoil drag (reverse flow), whereas the second case ($\kappa = 2$) there is a jet effect in the direction of flow that can be used profitably to propel the airfoil.

4.2 Free coupling regime

In this third example the same airfoil (NACA 2412, 105 panels) is now flexibly attached to a fixed point, as illustrated in Figure 1. Immersed in a uniform flow (V_∞, ρ), the airfoil is initially

removed from its position at rest ($w_o = 0.2\,m$ and $\theta_o = 8\,deg.$) until a stationary fluid state is reached. It is then relaxed to allow the fluid-structure coupling process to take place freely: it will be remarked that the mechanical energy decreases with time because of a transfer of energy to the fluid tracked in the form of a vortex wake. The point of this example is to look at the influence of the volumetric mass ρ on the convergence property of the FSI scheme, to show the severe limit observed for the classical coupling scheme (that we term CLAS), and finally to show the beneficial effect of the scheme corrected from the added mass effect (that we term CORR). Fluid flow conditions and structure characteristics are summarized in Table 1.

ρ	V_∞	m	$\mathcal{I}\vert_G$	K_Z	K_θ
$[kg/m^3]$	$[m/s]$	$[kg]$	$[kg/m^2]$	$[N/m]$	$[Nm/rad]$
$[1-2000]$	5	10	100	10^4	10^4

Table 1: Fluid flow conditions and structure properties

The estimated added mass matrix $[M_{add,e}]$ is calculated with equation (17) to obtain:

$$M_{add,e}(1,1) = 0.71\rho,\ M_{add,e}(1,2) = M_{add,e}(2,1) = -0.15rho,\ M_{add,e}(2,2) = 0.05\rho.$$

The airfoil is considered fixed over a given number of time steps n_{FIX}, then its flexibility is restored in order to start the free fluid-structure interaction. The time step Δt is related to the two natural frequencies, extracted from an eigenvalue analysis:

$$f_1 = \frac{1}{\tau_1} = 1.59\,Hz, \quad f_2 = \frac{1}{\tau_2} = 5.03\,Hz \quad \text{such as} \quad \Delta t = \frac{\min(\tau_1,\,\tau_2)}{200} \approx 10^{-3} s.$$

The same analysis, in accordance with equation (16), is conducted over $nstep$ time steps, for both the CLAS scheme (with $[M_{add,e}] = [0]$) and the CORR scheme, for a range of volumetric mass given in Table 1. For each time step, the number of iterations to convergence is extracted. Figure 5 illustrates the two calculations for the limit case $\rho = 21\,kg/m^3$. The upper graph shows the different wake patterns: black dots for CORR and larger, colored symbols for CLAS. With CLAS the wake pattern is seen to be wider, and the total number of iterations for convergence (lower graph) is systematically higher than with CORR.

This case corresponds to the limit observed for the CLAS scheme to converge. Any density above this value causes the coupling to diverge, as reported in Table 2. For the considered

$\rho\,[kg/m^3]$	1	10	20	25	100	1000	2000
# iterations (CLAS)	10	8	8	∞	∞	∞	∞
# iterations (CORR)	10	8	7	6	6	6	6

Table 2: Effect of density on the averaged total number of iterations for convergence

case, the CLAS scheme excludes densities higher than $20\,kg/m^3$. Above this value the coupling scheme systematically diverges. The CORR scheme, on the other hand, systematically converges, whatever the density value, which confirms its capacity to support heavy fluids. But the number of iterations is not the only determinant of whether a scheme is capable of converging. If the aerodynamic cœfficients are plotted with respect to time, it can clearly be seen that even where convergence is reached, the solution may not be physically acceptable. For $\rho \in [8,\,20]\,kg/m^3$ (not

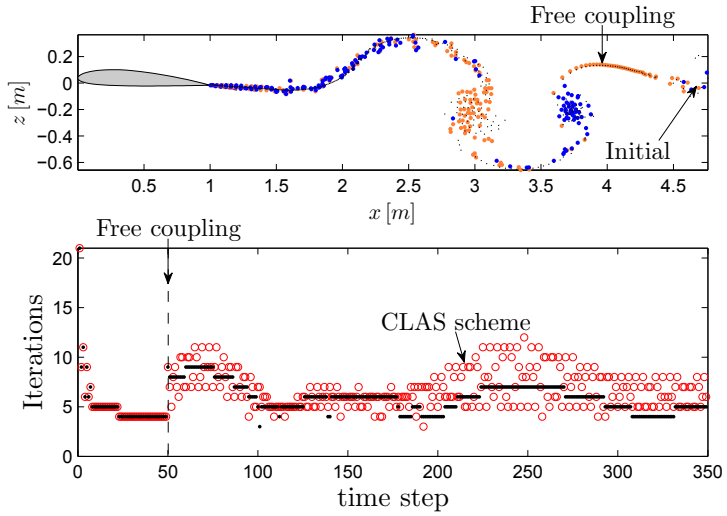

Figure 5: Convergence histories for CLAS and CORR schemes (case $\rho = 21\,kg/m^3$)

shown here) is can be observed (in the case of the CLAS coupling scheme) that all aerodynamic cœfficients oscillate and, second, that the drag coefficient C_D that ought to be null is in fact non-zero!

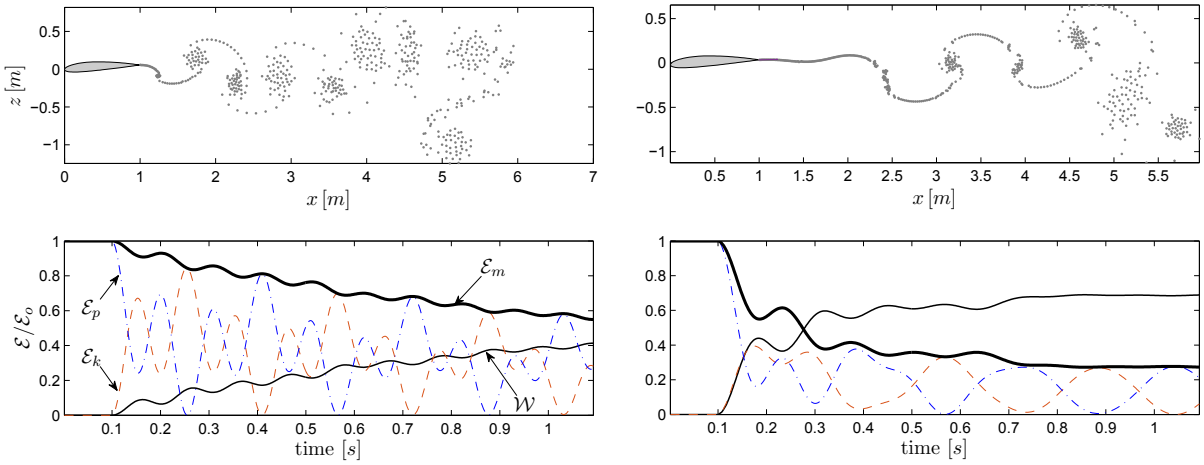

(a) $\rho = 1\,kg/m^3$ (b) $\rho = 10\,kg/m^3$

Figure 6: Dissipative effect due to airfoil energy transfer to the wake

The results below are solely obtained by using the CORR scheme. Figure 6(a) and (b) shows that increasing the fluid density gives rise to a predictable higher level of energy dissipation in the fluid, since a wake and vortex are generated that are simply convected downstream of the flow with their own energy (which the airfoil is consequently deprived of). Energy signals are normalized according to the initial energy $\mathcal{E}_o$ resulting from initial perturbations w_o and θ_o.

The two signals $\mathcal{E}_m$ and $\mathcal{W}$ have opposite behaviors, in agreement with the principle of energy conservation. In other words, an irreversible transfer of the mechanical energy $\mathcal{E}_m$ (equation 5) is observed between the main flow and the airfoil, due to the produced work $\mathcal{W}$. The higher the density, the higher the observed dissipative effect.

Figure 7 illustrates the frequency shifting observed and predicted for the two modes (pitching and plunging), directly related to the density value ρ (in log- scale). Theoretical predictions (solid lines), based on an eigenvalue analysis (mass, added mass and rigidity matrices), are compared with the observed frequencies extracted (symbols) from the FSI calculations after an FFT analysis.

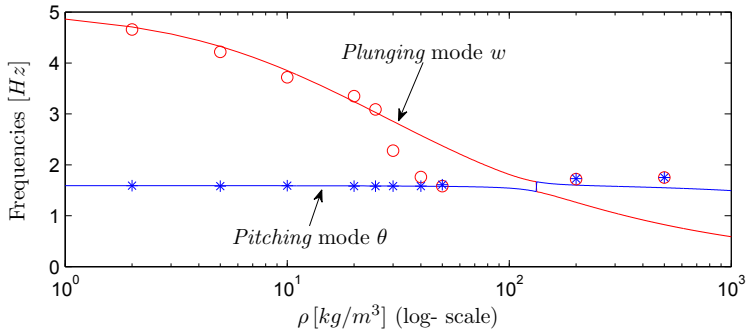

Figure 7: Modal frequencies with respect to ρ: predictions (lines) and FSI calculations (symbols)

It will be noted that the pitching frequency is relatively constant, whereas the plunging mode is quite sensitive to the value of the density. The eigenvalue analysis predicts a modal coalescing at the critical value $\rho_{coal} = 133\,kg/m^3$. The FSI simulations confirm the coalescing effect, but for $\rho = 50\,kg/m^3$.

5 Conclusions and prospects

This paper presents a corrected version of a strongly iterative partitioned FSI scheme for studying the dynamics of an airfoil flexibly attached and immersed in a heavy fluid. The intended application of our work mainly concerns the fluid-structure coupling that may operate between a moving lifting component (such as a marine current turbine) and a surrounding heavy fluid such as water. The mathematical model for the fluid is based on the potential Panel Method that offers the dual benefit of being restricted to a boundary element analysis and of ensuring the lifting capability of the component. The mathematical model for the structure, on the other hand, is based on the dynamics of a 2D airfoil that encounters plunging and pitching motions. We demonstrate that in simple case, the iterative convergence of a classical FSI partitioned scheme ceases to be guaranteed once the added mass exceeds the mass of the component. Correcting the FSI scheme to counteract the penalizing effect of the added mass allows convergence to be ensured, whatever the value of the added mass. The first example, for a forced oscillating airfoil, validates the fluid flow model for a stationary flow. The second example is intended to show how the classical FSI scheme is only applicable to a narrow range of fluids ($\rho \leq 8\,kg/m^3$), whereas taking into account the added mass effect on the coupling scheme can ensure the convergence required by coupling considerations. A coalescing and stable effect were observed, which also illustrates that the natural modes resulting from the flexibility of the structure may vary considerably. However, even though taking an estimated added mass matrix into account has obvious benefits in relation to FSI coupling in heavy fluids, this alone is not sufficient for accurately estimating the consequences of energy transfers that significantly modify the energy absorbed or dissipated by the system. We are currently looking at the possibility of

extending this approach to 3D applications to cover more realistic rotor geometries (wind mills, marine turbines), in order to establish the full requirements of FSI calculations for such devices.

REFERENCES

[1] M. Song, E. Lefrançois and M. Rachik. Development of a partitioned algorithm for fluid-structure coupling with no fluid density dependency. In *Computer & Fluids, DOI : 10.1016/j.compfluid.2013.05.022*, pp. 190-202, 2013

[2] Joseph Katz and Allen Plotkin, Low-Speed Aerodynamics, *Cambridge Aerospace Series, 2nd Edition*, 2001

[3] John J. Bertin and Russell M. Cummings, Aerodynamics for Engineers, *Pearson Edition, 6th Edition*, 2014

[4] Piperno S, Farhat C, Larrouturou B. Partitioned procedures for the transient solution of coupled aeroelastic problems. part I: Model problem, theory and two-dimensional application. *Comput. Methods Appl. Mech. Engrg. 124, pages 79-112*, 1995.

[5] Felippa CA, Park KC, Farhat C. Partitioned analysis of coupled mechanical systems. *Computer Methods in Applied Mechanics and Engineering, Vol. 190, Issues 24-25, 3247-3270* 2001.

[6] Idelsohn SR, Del Pin F, Rossi R, Oñate E. Fluid-structure interaction problems with strong added-mass effect. *International Journal for Numerical Methods in Engineering* 2009; **80**(10):1261–1294.

[7] van Brummelen E.H., Added mass effects of compressible and incompressible flows in fluid-structure interaction, *J. Appl. Mech.* 76 (2009), 021206-7.

[8] Fernández M. A., Gerbeau J.-F. and Grandmont C., A projection semi-implicit scheme for the coupling of an elastic structure with an incompressible fluid. *Int. J. Numer. Meth. Engng., 69 (4), pp.794-821* (2005)

[9] Küttler U., and Wall W., Fixed-point fluid-structure interaction solvers with dynamic relaxation, *Computational Mechanics* 43 (2008), no. 1, 61-72.

[10] A. Smith and J. Hess, Calculation of non-lifting potential flow about arbitrary three-dimensional bodies, *Technical Report E.S. 40622, Douglas Aircraft Company, Inc., Long Beach, CA*, 1962.

[11] T.Cebeci, M.Platzer, H.Chen, K.-C. Chang and J.P.Shao, Analysis of Low-Speed Unsteady Airfoil Flows, *Springer, Horizons Publishing*, 2005

[12] Currie, I. G., Fundamental Mechanics of Fluids, *Third edition, McGraw-Hill*,1993

[13] G. Dhatt, G. Touzot, E. Lefrançois, Finite Element Method, *Wiley-ISTE*, 2012

[14] C. E. Brennen, A review of added mass and fluid inertial forces, *Technical Report, Report Number CR 82.010. Contract Number N62583-81-MR-554*, 1982.